AIP Applied Physics Letters

Low-voltage driven ~1.54 μm electroluminescence from erbium-doped ZnO/p +-Si heterostructured devices: Energy transfer from ZnO host to erbium ions

Yang Yang, Yunpeng Li, Luelue Xiang, Xiangyang Ma, and Deren Yang

Citation: Applied Physics Letters **102**, 181111 (2013); doi: 10.1063/1.4804626
View online: http://dx.doi.org/10.1063/1.4804626
View Table of Contents: http://scitation.aip.org/content/aip/journal/apl/102/18?ver=pdfcov
Published by the AIP Publishing

Low-voltage driven ~1.54 μm electroluminescence from erbium-doped ZnO/p^+-Si heterostructured devices: Energy transfer from ZnO host to erbium ions

Yang Yang, Yunpeng Li, Luelue Xiang, Xiangyang Ma,[a] and Deren Yang
State Key Laboratory of Silicon Materials and Department of Materials Science and Engineering, Zhejiang University, Hangzhou 310027, People's Republic of China

(Received 8 March 2013; accepted 27 April 2013; published online 9 May 2013)

It is well known that the light emission at ~1.54 μm falls within the minimum loss window of silica optic fibers for optical communication and is of significance for the silicon-based optoelectronic integration. Herein, we report on erbium (Er)-related electroluminescence (EL) at ~1.54 μm from Er-doped ZnO (ZnO:Er)/p^+-Si heterostructured light-emitting devices. Such Er-related ~1.54 μm EL can be enabled at a voltage as low as 6 V. It is derived that the Er-related ~1.54 μm EL is triggered by transfer of the energy released from the defect-assisted indirect recombination in the ZnO host to the incorporated Er^{3+} ions. We believe that the present achievement paves the way for the Si-compatible ~1.54 μm light emitters using the cost-effective oxide semiconductors as the hosts of Er^{3+} ions. © *2013 AIP Publishing LLC*. [http://dx.doi.org/10.1063/1.4804626]

The light emission at ~1.54 μm is of significance, falling within the minimum loss window of silica optic fibers for optical communication. Moreover, it could be the standard optical source for the future optical interconnection in the silicon-based integrated circuits (ICs).[1–3] In this context, the light-emitting devices (LEDs) based on the erbium (Er)-doped silicon have been reported for over a decade.[4,5] Unfortunately, their light-emitting efficiencies are extremely low due to the low solubility of Er in silicon and low excitation efficiency of Er.[6] Afterwards, the LEDs based on Er-doped silicon oxide (SiO_x) or silicon nitride have been developed.[7–9] However, they are generally confronted with the difficulty in efficient electrical injection. Moreover, the ~1.54 μm LEDs based on Er-doped GaN on silicon have been fulfilled.[10–12] As is well known, GaN will encounter the scarcity of Ga resource in the long run. Addressing this point, we have recently reported the low-voltage driven electroluminescence (EL) from the Er-doped TiO_2/p^+-Si heterostructured devices, where the Er-related EL involves not only the ~1.54 μm emission but also the visible ones.[13,14] Generally, the original intention of using Er-doped semiconductors is to take advantage of the ~1.54 μm emission rather than the visible emissions related to the Er^{3+} ions. Therefore, how to disenable the visible EL from the Er^{3+} ions incorporated into the oxide semiconductors needs to be further addressed.

Considering the fact that the Er^{3+} ions incorporated into ZnO films generally exhibit only the ~1.54 μm emission at room temperature (RT),[15–20] in this work, we take advantage of such a feature of Er-doped ZnO (ZnO:Er) films, aiming to develop the ~1.54 μm LEDs. It is known that ZnO is an emerging oxide semiconductor with excellent optical properties in ultraviolet (UV) regime due to its wide bandgap of ~3.37 eV and large exciton binding energy of ~60 meV at RT.[21–23] In recent years, the ZnO-based optoelectronic devices including waveguide laser, random lasers, and various LEDs have been well demonstrated.[24–31] These devices generally emit light in the UV and visible regimes. In 2008, Harako *et al*. reported the visible and infrared (IR) EL from an *n*-ZnO:Er/*p*-Si heterostructure under reverse bias with a threshold voltage of ~10 V, which was ascribed to the impact ionization of Er^{3+} ions.[32] Recently, a proof-of-concept LED based on Si-rich ZnO:Er/p^+-Si heterostructure has been demonstrated, which exhibits detectable ~1.54 μm emission under forward bias with a threshold voltage of ~15 V.[33] In this device, the Si introduced into ZnO matrix is believed to contribute to the energy sensitization of Er-related emission. Despite the achievements as mentioned above, the realization of the Er-related EL only at ~1.54 μm from the ZnO:Er/Si heterostructured LEDs driven by low voltage (e.g., <10 V) is still a challenging subject, which is of significance for silicon-based optoelectronics.

In this work, we have realized low-voltage driven Er-related EL only at ~1.54 μm from the ZnO:Er/p^+-Si heterostructured LEDs under forward bias. The driven voltage for the onset ~1.54 μm EL is ~6 V. Such Er-related EL is triggered by the energy transfer from the ZnO host to the incorporated Er^{3+} ions. We believe that this work paves up the way for developing Si-compatible ~1.54 μm LEDs based on the Er-doped oxide semiconductors.

The ZnO:Er films were deposited by radio frequency magnetron sputtering on ⟨100⟩-oriented p^+-Si substrates with a resistivity of ~0.001 Ω cm. A ZnO ceramic target and an Er metallic target were used for co-sputtering. The sputter chamber was first evacuated to a base pressure of 3.5×10^{-3} Pa and was then inlet with Ar gas to a working pressure of 1.0 Pa. The sputtering power fed on the ZnO target was 70 W and that on the Er target was 25 or 35 W. During the sputtering, the p^+-Si substrate temperature was maintained at 100 °C. The sputtering proceeded for 30 min so that the sputtered films reached a thickness of ~160 nm. Such sputtered films were amorphous and oxygen deficient. They were then annealed at 700 °C for 2 h under O_2 ambient

[a]Author to whom correspondence should be addressed. Electronic mail: mxyoung@zju.edu.cn

to enable crystallization and a better stoichiometry. Moreover, this annealing process was favorable for the activation of Er^{3+} ions. For the formation of the LEDs based on the ZnO:Er/p^+-Si heterostructures, ~150 nm thick indium tin oxide (ITO) films were sputtered onto the ZnO:Er films and ~150 nm thick aluminum (Al) films were subsequently deposited on the backsides of p^+-Si substrates by electron beam evaporation. Herein, the ITO and Al films formed Ohmic contacts with the ZnO:Er films and p^+-Si substrates, respectively, acting as the device electrodes. They were patterned to be circular with a diameter of ~1.0 cm. The UV-visible and IR photoluminescence (PL) spectra were acquired by excitation using a 325 nm He-Cd laser and a Xe lamp with a spectrometer selected at 325 nm, respectively. The photoluminescence excitation (PLE) spectra were recorded using a Xe lamp as the excitation source. To activate EL from each LED as mentioned above, the forward direct-current bias was applied on the LED with the positive voltage connecting to the p^+-Si substrate. All the luminescence (PL and EL) spectra were measured at RT. The UV-visible and IR luminescence spectra were recorded using Acton SpectraPro 2500i and Edinburgh FLS920P Spectrometers, respectively.

The atomic composition of the ZnO:Er films were characterized by Rutherford backscattering spectroscopy (RBS) using 2.022 MeV ^{4}He ion beam at a scattering angle of 165°. It is derived that the molar ratios of Er/Zn are 0.9 and 1.7% in the two ZnO:Er films prepared with the feeding powers of 25 and 35 W on the Er target, respectively. For the sake of simplicity, hereafter, the two ZnO:Er films will be denoted as ZnO:Er (0.9%) and ZnO:Er (1.7%) films, correspondingly. Fig. 1(a) shows the X-ray diffraction (XRD) patterns of two different ZnO:Er films annealed at 700 °C for 2 h under O_2 ambient. As can be seen, there are only the pronounced peaks corresponding to the (002) and (103) planes of hexagonal ZnO in each XRD pattern. The fact that no Er-related phases are revealed in the XRD patterns indicates that the Er^{3+} ions are substantially incorporated into the ZnO host, existing in both the grains and grain boundaries. Note, Fig. 1(a), that the XRD peak intensities of the ZnO:Er (0.9%) film are stronger than those of the ZnO:Er (1.7%) film. Considering that the two ZnO:Er films have almost the same thickness, it is believed that the ZnO:Er (0.9%) film has relatively better crystallinity. Since the ionic radius of Er^{3+} ion (0.88 Å) is larger than that of Zn^{2+} ion (0.74 Å), more significant substitution of Er^{3+} ions for the Zn lattices leads to the degradation of the crystallinity of ZnO host.

The microstructure and composition of the ZnO:Er (1.7%) film were further characterized by high resolution transmission electron microscopy and energy dispersive X-ray spectroscopy (HRTEM and EDS). The HRTEM image of the ZnO:Er (1.7%) film sputtered on the p^+-Si substrate is displayed in Fig. 1(b). As can be seen, there is a 3–5 nm thick amorphous layer, which is generally believed to be of SiO_x ($x \leq 2$) in composition, between the silicon substrate and the ZnO:Er film. It should be mentioned that no crystal grains of Er_2O_3 and other Er-related phase can be found in the HRTEM image, which is in accord with the result of XRD characterization. The quantitative EDS analyses have been performed on the ZnO grains and on the areas across the grain boundaries. In comparison, the average content of Er (~2.2% in molar ratio of Er/Zn) in the areas across the grain boundaries is a little larger than that (~1.4%) inside the ZnO grains. Evidently, this fact accounts for the impurity segregation effect of grain boundaries. Moreover, the Er^{3+} ions incorporated into the ZnO grains are believed to be substitute for the Zn lattice sites. By the way, it is understandable that the amount of the Er^{3+} ions incorporated into the ZnO grains should be larger in the ZnO:Er (1.7%) film than in the ZnO:Er (0.9%) one.

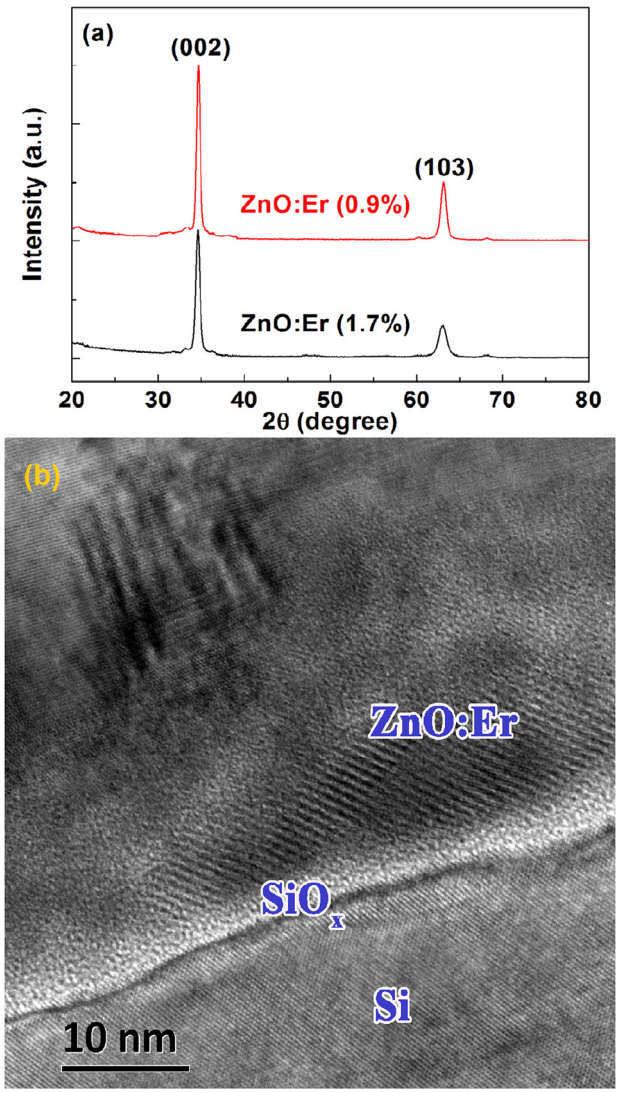

FIG. 1. (a) XRD patterns of the ZnO:Er films with different Er contents, annealed at 700 °C for 2 h under O_2 ambient. (b) A representative HRTEM image of the ZnO:Er (1.7%) film on a silicon substrate, annealed at 700 °C for 2 h under O_2 ambient.

Fig. 2(a) shows the UV-visible and IR PL spectra of the ZnO:Er (1.7%) and ZnO:Er (0.9%) films, excited by the 325 nm light. Therein, the emission bands peaking at ~380 nm correspond to the near-band-edge (NBE) emission of ZnO and the broad emission bands covering from 450 to 700 nm are believed to relate to the deep-level defects such as oxygen vacancies or zinc interstitials in the ZnO host. Noteworthily, there are no discernable sharp peaks related to the visible emissions from the Er^{3+} ions, which is in consistent with other reports.[32,33] While, in the IR region, the ~1.54 μm emissions

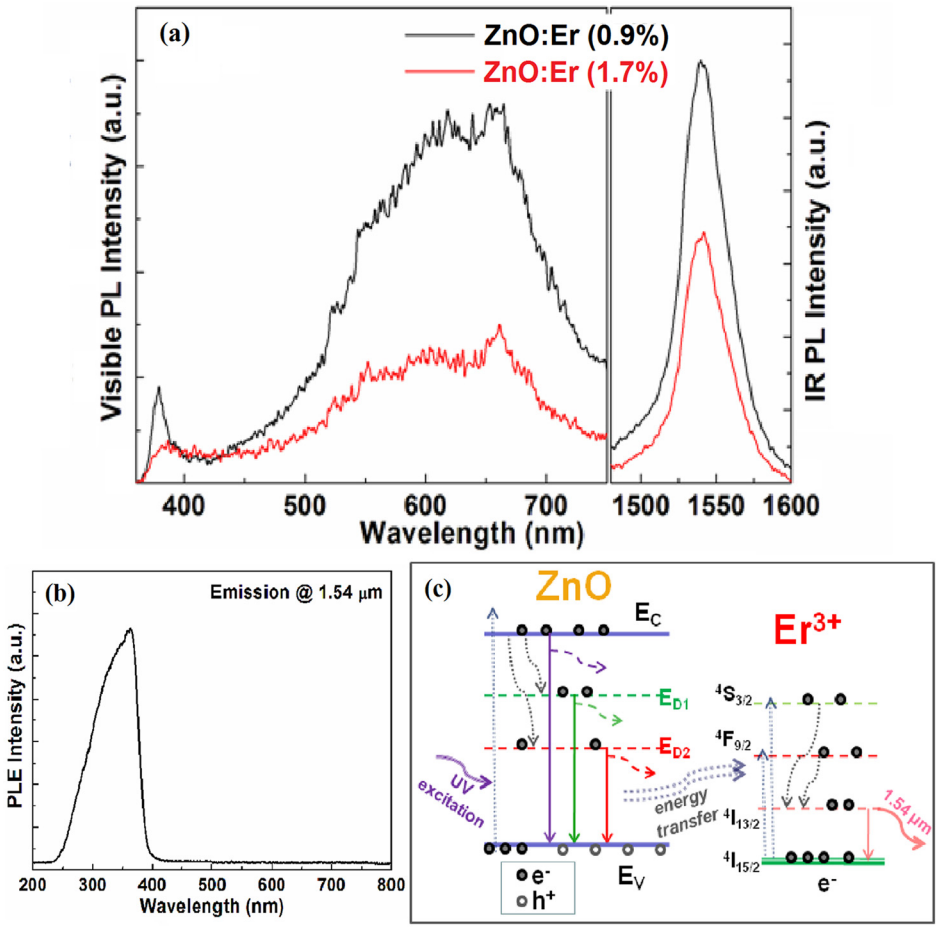

FIG. 2. (a) PL spectra for the ZnO:Er films with different Er contents, annealed at 700 °C for 2 h under O_2 ambient. (b) PLE spectrum monitoring the emission at ~1.54 μm for the ZnO:Er (0.9%) film annealed at 700 °C for 2 h under O_2 ambient. (c) Schematic diagram for the proposed energy transfer process in the case of PL from the ZnO:Er film.

assigned to the $^4I_{13/2} \rightarrow {}^4I_{15/2}$ transition in the Er^{3+} ions occur substantially in both ZnO:Er films. Overall, the ZnO:Er (1.7%) film exhibits much weaker PL than the ZnO:Er (0.9%) film. As mentioned above, the former is inferior to the latter in terms of the crystallinity, thus having much more non-radiative recombination centers. Therefore, it is understandable that the ZnO-host-related UV and visible emissions from the ZnO:Er (1.7%) film are relatively weaker. The weaker Er-related ~1.54 μm emission from the ZnO:Er (1.7%) film with respect to that from the ZnO:Er (0.9%) film indicates the apparent concentration quenching. Moreover, this could be related to some Er clustering in the ZnO:Er (1.7%) film, which needs to be clarified in the future work.

The PLE spectrum monitoring the emission at ~1.54 μm for the ZnO:Er (0.9%) film, as shown in Fig. 2(b), indicates that there is only one excitation peak at ~370 nm, a little bit shorter than the wavelength corresponding to the bandgap of ZnO. Consistently, no resonant visible absorption peaks related to the Er^{3+} ions appear in the UV-Vis absorption spectra (not shown herein). The presence of the ~1.54 μm PL from the Er^{3+} ions under the non-resonant excitation condition, as shown in Fig. 2(a), evidences the efficient energy transfer between the ZnO host and the Er^{3+} ions. The ~1.54 μm emission dynamics of ZnO:Er film at a low temperature of 20 K, investigated by Komuro *et al.*, indicates that this emission can be achieved either by exciting indirectly Er^{3+} ions due to an electron-hole-mediated process in the ZnO host or by exciting directly discrete energy levels of Er^{3+} ions. Moreover, the indirect excitation efficiency is superior to the direct one.[34,35] However, as mentioned above, our RT PLE spectrum does not reveal the direct excitation of Er^{3+} ions. This is due to the remarkable temperature quenching of the direct excitation process occurring in the Er^{3+} ions incorporated into ZnO. Actually, our result again confirms that the indirect excitation originated from the ZnO host is more efficient than the direct excitation of Er^{3+} ions. Fig. 2(c) shows the schematic diagram for the proposed energy transfer from the ZnO host to the incorporated Er^{3+} ions. Under the UV excitation, electrons in the valence band of ZnO are excited to the conduction band, leaving holes in the valence band. In the de-excitation process, a part of electrons directly recombine with holes in the valence band. This direct electron-hole recombination features extremely short lifetime because ZnO is a direct bandgap semiconductor. Therefore, the transfer of the energy released from the direct recombination of carriers in the ZnO host to the Er^{3+} ions is negligible. Actually, the released energy is substantially converted into the NBE emission of ZnO, as manifested by the UV band peaking at ~380 nm, as shown in Fig. 2(a). Besides, other excited electrons in the conduction band of ZnO firstly fall into the defect-related states and then drop down to the valence band to recombine with holes therein. Such indirect recombination of carriers in the ZnO host, on one hand, gives rise to the visible emissions and, on the other hand, resonantly transfers energy to the Er^{3+} ions nearby the defects. As can be known from the PL spectra shown in Fig. 2(a), the defect-assisted indirect recombination of carriers in the ZnO host releases the energy covering the visible

spectral range. Therefore, the aforementioned energy transfer can essentially trigger the excitations of $^4I_{15/2} \rightarrow {}^4S_{3/2}$ and $^4F_{9/2}$ (corresponding to the wavelengths of ~554 and 667 nm, respectively) in the Er^{3+} ions. Then the excited intra-4*f* electrons of Er^{3+} ions further go through a nonradiative relaxation to the first excited level $^4I_{13/2}$. The following de-excitation transition to the ground level $^4I_{15/2}$ results in the ~1.54 μm emission.

Fig. 3(a) shows the EL spectra acquired at the same injection current for the ZnO:Er/p^+-Si heterostructured devices using the ZnO:Er (1.7%) and ZnO:Er (0.9%) films, respectively. Again, the UV and visible bands are ascribed to the NBE and defect-related emissions from the ZnO host, respectively. While, the ~1.54 μm emission originates from the $^4I_{13/2} \rightarrow {}^4I_{15/2}$ transition in the Er^{3+} ions. As can be seen, the device using the ZnO:Er (0.9%) film exhibits much stronger EL than the counterpart using the ZnO:Er (1.7%) film in the whole spectrum. Apparently, this contrast between the EL intensities of the two devices is in accord with the case of PL, as shown in Fig. 2(a), for the two ZnO:Er films. Fig. 3(b) further shows the evolution of EL spectra with increasing injection current for the ZnO:Er/p^+-Si heterostructured device using the ZnO:Er (0.9%) film. Obviously, the EL intensity increases with the injection current.

The current-voltage (*I-V*) characteristic of the ZnO:Er(0.9%)/p^+-Si heterostructured device is shown in Fig. 3(c), indicating non-rectifying behavior. Herein, the forward/reverse bias refers to that the positive/negative voltage is connected to p^+-Si substrate. However, the devices are electroluminescent only under the forward bias, indicating that the simultaneous injection of electrons and holes is necessary for the EL. Moreover, as shown in Fig. 3(b), the driven voltage for the Er-related ~1.54 μm EL is fairly low. Actually, such voltage is essentially assumed by the intermediate SiO_x layer between the ZnO:Er film and the p^+-Si substrate. In other words, the voltage dropping across the ZnO:Er film and therefore the resulting electrical field is considerably low. Considering the above-mentioned two aspects, it is believed that the Er-related EL at ~1.54 μm is ascribed to the carrier-recombination-mediated energy transfer mechanism rather than the direct impact excitation of Er^{3+} ions.

Fig. 4 illustrates the schematic diagram for the energy band structure of the ZnO:Er/p^+-Si heterostructured device under sufficient forward bias and the proposed energy transfer from the ZnO host to the Er^{3+} ions. Under the forward bias, the energy band of ZnO bends downward nearby the ZnO/SiO_x interface, while that of Si bends upward nearby the Si/SiO_x interface. At a sufficiently high forward bias voltage, a considerable amount of holes accumulated in the region adjacent to the Si/SiO_x interface will tunnel through the SiO_x layer into the valence band of ZnO. In the ZnO host, a part of electrons in the conduction band directly recombine with holes in the valence band, generating the UV emission. While, other electrons in the conduction band of ZnO first transit to the defect-related energy levels and then recombine with holes in the valence band. Just like the scenario occurring in the PL of ZnO:Er film, the indirect

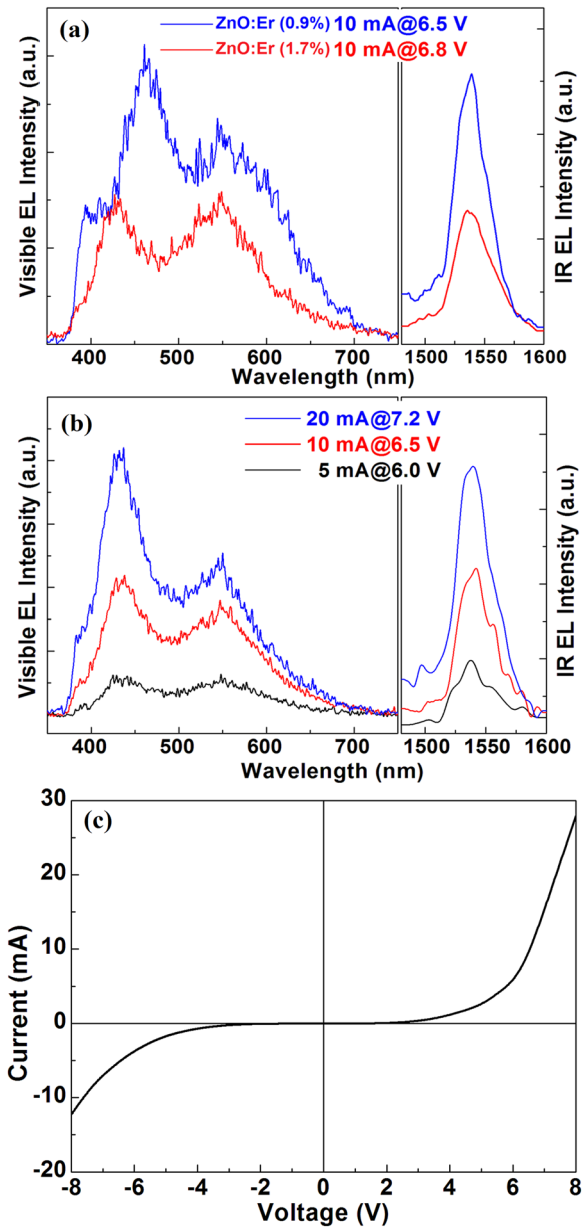

FIG. 3. (a) EL spectra acquired with the same injection current for the ZnO:Er/p^+-Si heterostructured devices using the ZnO:Er films with different Er contents. (b) EL spectra for the ZnO:Er(0.9%)/p^+-Si heterostructured device under different injection currents. (c) The *I-V* characteristic of the ZnO:Er(0.9%)/p^+-Si heterostructured device.

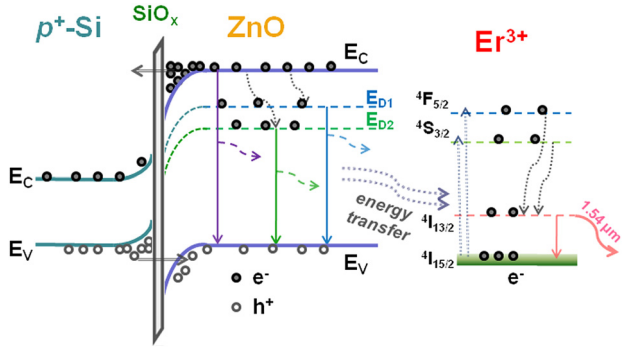

FIG. 4. Schematic diagram for the energy band structure of the ZnO:Er/p^+-Si heterostructured device under forward bias and the transfer of energy released from the defect-assisted indirect recombination in the ZnO host to the incorporated Er^{3+} ions, accompanied with the excitation and de-excitation processes occurring in the Er^{3+} ions.

recombination of carriers in the ZnO host, on one hand, enables the visible EL and, on the other hand, resonantly transfer energy to the incorporated Er^{3+} ions nearby the defects to trigger the excitations of $^4I_{15/2} \rightarrow {}^4S_{3/2}$ and $^4F_{5/2}$. The following de-excitation process is terminated with the radiative transition of $^4I_{13/2} \rightarrow {}^4I_{15/2}$, which leads to the $\sim$1.54 μm emission.

In summary, we have definitely demonstrated the low-voltage driven $\sim$1.54 μm EL from the ZnO:Er/p^+-Si heterostructured LEDs with the ZnO:Er films annealed at 700 °C. The ZnO:Er films exhibit single ZnO phase in view of XRD and HRTEM characterizations. The incorporated Er^{3+} ions partly reside in the ZnO grains, leaving others aggregated at the grain boundaries without forming detectable Er_2O_3 phase. Under sufficiently high forward bias, the ZnO:Er/p^+-Si heterostructured LEDs exhibit remarkable $\sim$1.54 μm EL from the Er^{3+} ions besides the UV and visible emissions from the ZnO host. It is believed that the energy transferred from the defect-assisted indirect recombination of the carries in the ZnO host excites the Er^{3+} ions close to the defects and the subsequent de-excitation process gives rise to the $\sim$1.54 μm emission. We believe that this work sheds light on the development of silicon-based $\sim$1.54 μm LEDs using the Er-doped oxide semiconductors.

The authors would like to thank the financial supports from "973 Program" (2013CB632102), National Science Foundation of China (No. 61176042), Zhejiang provincial Natural Science Fund (R4090055), Innovation Team Project of Zhejiang Province (2009R50005).

[1]N. Daldosso and L. Pavesi, Laser Photon. Rev. **3**, 508 (2009).
[2]R. Li, S. Yerci, and L. D. Negro, Appl. Phys. Lett. **95**, 041111 (2009).
[3]O. Jambois, F. Gourbilleau, A. J. Kenyon, J. Montserrat, R. Rizk, and B. Garrido, Opt. Express. **18**, 2230 (2010).
[4]G. Franzo, F. Priolo, S. Coffa, A. Polman, and A. Carnera, Appl. Phys. Lett. **64**, 2235 (1994).
[5]F. Priolo, G. Franzo, D. Pacifici, V. Vinciguerra, F. Iacona, and A. Irrera, J. Appl. Phys. **89**, 264 (2001).
[6]A. J. Kenyon, Semicond. Sci. Technol. **20**, R65 (2005).
[7]I. Izeddin, D. Timmerman, T. Gregorkiewicz, A. Z. Moskalenko, A. A. prokofiev, I. N. Yassievicha, and M. Fujii, Phys. Rev. B. **78**, 035327 (2008).
[8]A. Kanjalal, L. Rebohle, W. Skorupa, and M. Helm, Appl. Phys. Lett. **94**, 101916 (2009).
[9]A. Irrera, F. Iacona, G. Franzo, M. Miritello, R. L. Savio, M. E. Castagna, S. Coffa, and F. Priolo, J. Appl. Phys. **107**, 054302 (2010).
[10]M. Garter, J. Scofield, R. Birkhahn, and A. J. Steckl, Appl. Phys. Lett. **74**, 182 (1999).
[11]J. M. Zavada, S. X. Jin, N. Nepal, J. Y. Lin, H. X. Jiang, P. Chow, and B. Hertog, Appl. Phys. Lett. **84**, 1061 (2004).
[12]R. Dahal, C. Ugolini, J. Y. Lin, H. X. Jiang, and J. M. Zavada, Appl. Phys. Lett. **97**, 141109 (2010).
[13]Y. Yang, L. Jin, X. Y. Ma, and D. R. Yang, Appl. Phys. Lett. **100**, 031103 (2012).
[14]Y. Yang, Y. Li, L. Jin, X. Y. Ma and D. Yang, Appl. Phys. Lett. **102**, 021108 (2013).
[15]M. Kohls, M. Bonanni, L. Spanhel, D. Su, and M. Giersig, Appl. Phys. Lett. **81**, 3858 (2002).
[16]A. K. Pradhan, L. Douglas, H. Mustafa, R. Mundle, D. Hunter, and C. E. Bonner, Appl. Phys. Lett. **90**, 072108 (2007).
[17]J. H. Lang, X. Li, J. H. Yang, L. L. Yang, Y. J. Zhang, Y. S. Yan, Q. Han, M. B. Wei, M. Gao, X. Y. Liu, and R. Wang, Appl. Surf. Sci. **257**, 9574 (2011).
[18]Y. R. Jang, K. H. Yoo, J. S. Ahn, C. Kim, and S. M. Park, Appl. Surf. Sci. **257**, 2822 (2011).
[19]D. Kouyate, J. C. Ronfardharet, and J. Kossanyi, J. Lumin. **50**, 205 (1991).
[20]N. Mais, J. P. Reithmaier, A. Forchel, M. Kohls, L. Spanhel, and G. Muller, Appl. Phys. Lett. **75**, 2005 (1999).
[21]M. Abdullah, T. Morimoto, and K. Okuyama, Adv. Funct. Mater. **13**, 800 (2003).
[22]U. Ozgur, Y. I. Alivov, C. Liu, A. Teke, M. A. Reshchikov, S. Dogan, V. Avrutin, S. J. Cho, and H. Morkoc, J. Appl. Phys. **98**, 041301 (2005).
[23]H. K. Fu, C. L. Cheng, C. H. Wang, T. Y. Lin, and Y. F. Chen, Adv. Funct. Mater. **19**, 3471 (2009).
[24]S. Chu, G. P. Wang, W. H. Zhou, Y. Q. Lin, L. Chernyak, J. Z. Zhao, J. Y. Kong, L. Li, J. J. Ren, and J. L. Liu, Nat. Nanotechnol. **6**, 506 (2011).
[25]P. L. Chen, X. Y. Ma, and D. R. Yang, Appl. Phys. Lett. **89**, 111112 (2006).
[26]H. K. Liang, S. F. Yu, and H. Y. Yang, Appl. Phys. Lett. **97**, 241107 (2010).
[27]J. H. Lim, C. K. Kang, K. K. Kim, I. K. Park, D. K. Hwang, and S. J. Park, Adv. Mater. **18**, 2720 (2006).
[28]X. Y. Ma, P. L. Chen, D. S. Li, Y. Y. Zhang, and D. R. Yang, Appl. Phys. Lett. **91**, 251109 (2007).
[29]X. Y. Ma, J. W. Pan, P. L. Chen, D. S. Li, H. Zhang, Y. Yang, and D. R. Yang, Opt. Express. **17**, 14426 (2009).
[30]Y. P. Li, X. Y. Ma, M. S. Xu, L. L. Xiang, and D. R. Yang, Opt. Express **19**, 8662 (2011).
[31]O. Lupan, T. Pauporte, T. L. Bahers, B. Vianaa, and I. Ciofini, Adv. Funct. Mater. **21**, 3564 (2011).
[32]S. Harako, S. Yokoyama, K. Ide, X. Zhao, and S. Komoro, Phys. Status. Solidi. A **205**, 19 (2008).
[33]E. F. Pecora, T. I. Murphy, and L. D. Negro, Appl. Phys. Lett. **101**, 191115 (2012).
[34]S. Komuro, T. Katsumata, T. Morikawa, X. Zhao, H. Isshiki, and Y. Aoyagi, Appl. Phys. Lett. **76**, 3935 (2000).
[35]S. Komuro, T. Katsumata, T. Morikawa, X. W. Zhao, H. Isshiki, and Y. Aoyagi, J. Appl. Phys. **88**, 7129 (2000).